nanomaterials

MDPI

Article

Fe_3O_4Nanoparticles Loaded on Lignin Nanoparticles Applied as a Peroxidase Mimic for the Sensitively Colorimetric Detection of H_2O_2

Qingtong Zhang [1,2], Mingfu Li [1,2], ChenyanGuo [1,2], ZhuanJia [1,2], Guangcong Wan [1,2], Shuangfei Wang [1,2] and Douyong Min [1,2,*]

[1] College of Light Industry and Food Engineering, Guangxi University, Nanning 530004, China; qingyutong110@163.com (Q.Z.); mingfuli@mail.gxu.cn (M.L.); guochenyan2017@163.com (C.G.); jiazhuan123@163.com (Z.J.); wanguangcong@163.com (G.W.); wangsf@gxu.edu.cn (S.W.)

[2] Guangxi Key Lab of Clean Pulp & Papermaking and pollution Control, Nanning 530004, China

* Correspondence: mindouyong@gxu.edu.cn

Received: 28 January 2019; Accepted: 1 February 2019; Published: 6 February 2019

Abstract: Lignin is the second largest naturally renewable resource and is primarily a by-product of the pulp and paper industry; however, its inefficient use presents a challenge. In this work, Fe_3O_4 nanoparticles loaded on lignin nanoparticles (Fe_3O_4@LNPs) were prepared by the self-assembly method and it possessed an enhanced peroxidase-like activity. Fe_3O_4@LNPs catalyzed the oxidation of 3,3',5,5'-tetramethylbenzidine (TMB) in the presence of H_2O_2 to generate a blue color, was observable by the naked eye. Under the optimal conditions, Fe_3O_4@LNPs showed the ability of sensitive colorimetric detection of H_2O_2within a range of 5–100 μM and the limit of detection was 2 μM. The high catalytic activity of Fe_3O_4@LNPs allows its prospective use in a wide variety of applications, including clinical diagnosis, food safety, and environmental monitoring.

Keywords: Fe_3O_4 nanoparticles; Lignin nanoparticles; peroxidase mimic; colorimetric; H_2O_2 detection

1. Introduction

Hydrogen peroxide (H_2O_2), as one of the most important reactive oxygen species (ROS), is widely used in the food and chemical industries, clinical medicine, and environmental monitoring [1–3]. Studies have shown that long-term exposure to H_2O_2 can cause serious harm to a person's health, including poisoning, respiratory inflammation [4], cancer, Alzheimer's disease, and Parkinson's disease [5]. Therefore, the substantial research efforts are devoted to develop methods for the detection of H_2O_2,such ashigh-performance liquid chromatography (HPLC) [6], electrochemistry [1], spectrometry [7], chemiluminescence [8], and colorimetric assays [9]. HPLC, electrochemistry, and chemiluminescence methods are sensitive, but their processes are complex and time-consuming. Spectrometry has the advantage of a simple and low-cost operation but exhibits the disadvantage of poor sensitivity. At present, colorimetric assay methods have been garnering attention due to their high sensitivity and simplicity. Furthermore, colorimetric assay results can be observed unaided and without the use of any sophisticated instruments. Horseradish peroxidase (HRP) is commonly used as a catalyst in conventional colorimetric assay methods to obtain the color signal. As a natural enzyme, HRP is easily affected by acidity, temperature, and inhibitors. In addition, the high cost associated with its preparation, purification and extreme storage conditions also inevitably limits its widespread application [10].

Since the first report of Fe_3O_4 nanoparticles (Fe_3O_4 NPs) possessing peroxidase-like activity [11], many other nanomaterials, including CeO_2 nanoparticles [12], NiO_2 nanoparticles [13]and MnO_2 nanosheets [14], have also demonstrated intrinsic peroxidase-like activity. These metal nanomaterials are low-cost, sensitive, and maintain their activities in a relatively wide range of environmental conditions, but they all present the problem of agglomeration [15]. To tackle this problem, researchers use graphene or graphene oxide as a structural support to prevent these metal nanomaterials from aggregating in solution [16,17]. However, the high cost of graphene and graphene oxide seriously restricts the widespread application of metal nanozymes.

Lignin is the second most abundant organic macromolecular compound from biomass after cellulose [18]. The primary structure of lignin is composed of three different phenylpropane monomer units: guaiacyl (G), syringyl (S), and p–hydroxyphenol (H) units [19]. These monomer units are mainly linked by ether bonds (β-O-4, 4-O-5, α-O-4, α-O-γ, etc.) and carbon-carbon bonds (β-β，β-1，β-5, 5-5，β-6, etc.) [20,21]. A proposed structural diagram of lignin is shown in Figure 1. Similar to graphene oxide, lignin molecules contain many functional groups, such as hydroxyl and carboxyl groups, which offers the possibility of a stable dispersion of lignin-based materials in aqueous solutions. Recent studies showed that lignin-based nanoparticles can disperse stably in aqueous solutions [18]. Therefore, metal nanozymes carried by lignin nanoparticles can be stably dispersed in solution. Nevertheless, the literature contains few reports of lignin nanoparticles being used to enhance the dispersity of metal nanozymes in the colorimetric detection of H_2O_2.

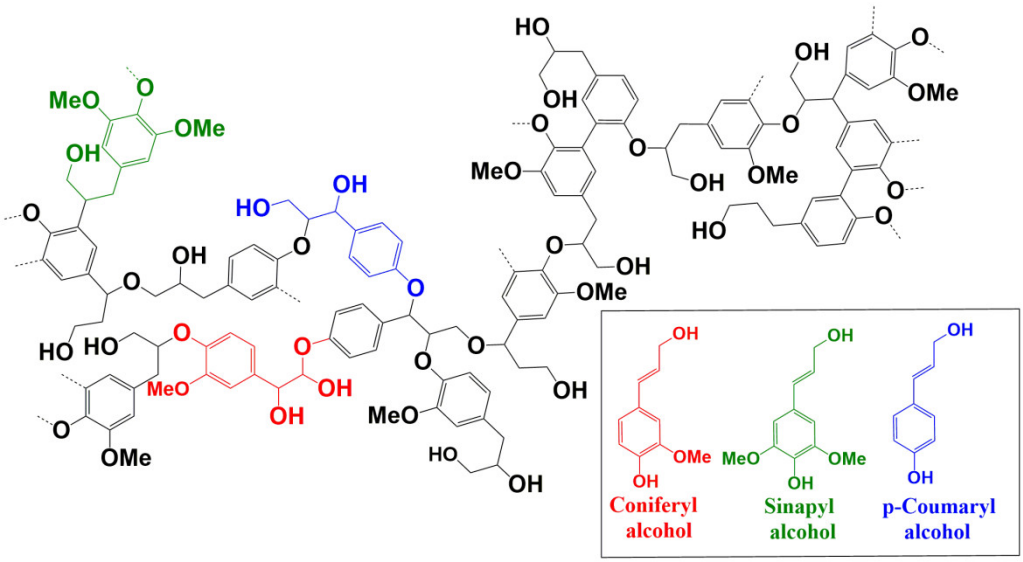

Figure 1. The proposed structure of lignin. Inset: three primary units of lignin.

As a common mimetic enzyme of horseradish peroxidase, Fe_3O_4 NPs have high catalytic activity and stability during reactions [22]. However, Fe_3O_4 NPs also present the urgent problem of agglomeration in solution. In this work, we explored the influence of the preparation conditions on the morphology of Fe_3O_4@LNPs. Then, Fe_3O_4 NPs loaded on lignin nanoparticles (Fe_3O_4@LNPs) were prepared. The prepared Fe_3O_4@LNPs exhibited excellent dispersion stability in water and showed higher catalytic activity than Fe_3O_4 NPs. The prepared Fe_3O_4@LNPs effectively catalyzed H_2O_2 to generate hydroxyl radicals, followed by the oxidation of 3,3',5,5'-tetramethylbenzidine (TMB) [23]. The oxidized TMB had a characteristic absorbance at 652 nm [24]. Therefore, in the presence of H_2O_2, TMB, and Fe_3O_4@LNPs as catalyst, the reaction system changed from colorless to blue that was identified by the naked eye or quantified by UV-vis spectrophotometer. Because of its excellent dispersion stability in aqueous solution and sensitive peroxidase-like catalytic activity, Fe_3O_4@LNPs can be used in a diverse set of applications.

2. Experimental

2.1. Materials and Reagents

Spruce chips were obtained from a Swedish farm. Tetrahydrofuran (THF), Fe_3O_4 NPs (average diameters: 20–30 nm), and TMB were purchased from Aladdin Industrial Co., Ltd. (Shanghai, China). The other analytical grade chemicals were purchased from Boyu Chemicals Company (Nanning, Guangxi, China), and were used without further purification.

The chips were cooked in a pressure vessel under the following conditions: the total titratable alkali value was 26%, the sulfidity was 20%, the solid-to-liquid ratio was 1:4, a residence time was 4.5 h, and the temperature was 165 °C. When the cooking was completed, the separated black liquor was adjusted to pH = 2 with 2 M H_2SO_4while stirring to precipitate lignin. After standing for 3 h, the supernatant was removed. After centrifugation, washing, and freeze-drying, the crude Kraft lignin was obtained. The crude Kraft lignin was dissolved in THF and stirred for 30 min; the undissolved material was removed by filtering through a 0.45 μm organic filter membrane (Pall Scientific, New York, NY, USA). The lignin/THF solution was stirred under the fume hood until the THF evaporated completely. Then, the powder was dried at 40 °C under vacuum for 48 h to obtain the purified Kraft lignin.

2.2. Statistical Analysis

All the experiments were performed in triplicate, and the averaged values were reported in this study.

2.3. Preparation of Fe_3O_4@LNPs

The purified lignin was dissolved in THF to prepare solutions of 0.5, 1.0, and 5.0, mg/mL. With vigorous mechanical stirring, 0.1 mg/mL Fe_3O_4 NPs suspension was added dropwise to the lignin/THF solutions using a microsyringe until the suspension with 20% consistency was obtained. The suspension was stirred for an additional 20 min to evaporate THF. Then, the suspension was transferred into a dialysis bag (MWCO: 6000, Union Carbide, Connecticut, CT, USA) and immersed in an excess of deionized water to remove the residual THF. Little trace of THF was detected after 24 h dialysis. Then, the suspension was centrifuged to achieve the solid part which was freeze-dried to obtain Fe_3O_4@LNPs. Fe_3O_4@LNPs prepared from the solution with 0.5, 1.0, and 5.0 mg/mL initial lignin concentration was respectively denoted as L_1, L_2, and L_3.

2.4. Peroxidase-Like Activity of Fe_3O_4@LNPs

The peroxidase-like activity of Fe_3O_4@LNPs was investigated by catalytically oxidizing TMB in the presence of H_2O_2.The concentrations of TMB and H_2O_2were respectively 4 mM and 100 mM, 0.1 M Citric acid-disodium hydrogen phosphate solution (CPBS) (pH = 3.0) was applied as the buffer, and the final volume of the mixture was 3 mL. The mixture was incubated at 50 °C for 30 min. As for the blank experiments, Fe_3O_4@LNPs was replaced by LNPs (lignin nanoparticles) or Fe_3O_4 NPs to complete the reaction under the same conditions. The oxidized TMB had a maximum absorbance at 652 nm [25].Therefore, the peroxidase-like activity of Fe_3O_4@LNPs was evaluated through changes of the solution color and the absorbance at 652 nm.

2.5. Steady Kinetic Analysis of Fe_3O_4@LNPs

The steady-state kinetic measurements were carried out to investigate the mechanism of the peroxidase-like activity of Fe_3O_4@LNPs at room temperature. Approximately 600 μL of Fe_3O_4@LNPs （264 μg/mL） was mixed with 1.8 mL CPBS (0.1 M, pH = 3.0). As for the first experiment, 300 μL H_2O_2(100 mM) was used, while the TMB concentration was varied (0.4, 0.6, 0.8, 1.0, 1.5, 2.0, 3.0, 4.0 and 6.0 mM). As for the second experiment, 300 μL TMB (4.0 mM) was used, while the concentration of H_2O_2 was varied (10, 15, 25, 30, 50, 100, 150, and 250 mM). TheMichaelis-Menten constant was calculated from the Lineweaver-Burk double reciprocal plot by the following equation: $1/v = K_m/v_m(1/[S] + 1/K_m)$, where v is the initial velocity, K_m is the Michaelis constant, v_m is the maximum reaction rate, and [S] is the concentration of substrate [26].

2.6. Colorimetric Detection of H_2O_2

For the colorimetric analysis of H_2O_2, 600 μL Fe_3O_4@LNPs (264 μg/mL), 300 μL of TMB (4 mM) and 300 μL H_2O_2 (different concentrations) were mixed with 1.8 mL CPBS (0.1 M, pH = 3.0). The mixed solution was incubated at 50 °C for 30 min. The absorbance of the resulted sample measured by a UV-visible spectrophotometer at 652 nm was used to generate the standard curve for the detection of H_2O_2.

The limit of detection (LOD) of H_2O_2 was calculated based on previous literature [27] via the following equation: LOD = 3S/M, where S is the standard deviation of blank samples and M is the slope of the linear curve between the absorbance at 652 nm and H_2O_2 concentration. Eleven blank experiments were carried out as follows: 600 μL Fe_3O_4@LNPs (264 μg/mL), 300 μL of TMB (4 mM) and the corresponding volume (300 μL) of H_2O replacing H_2O_2 were mixed with 1.8 mL CPBS (0.1 M, pH = 3.0). The mixtures were incubated at 50 °C for 30 min. The absorbance of 11 blank experiments at 652 nm was collected to calculate S value.

2.7. Characterization

The ^{31}Pnuclear magnetic resonance (NMR) spectrum of lignin was acquired on an NMR spectrometer (AVANCE III 500 MHz, Bruker, Germany). The morphologies and element analysis of Fe_3O_4@LNPs were recorded by field emission transmission electron microscope (FE-TEM) (Tecnail G2F20, FEI Company, Hillsboro, OR, USA) with an accelerating voltage of 200 KV. UV-vis spectra were recorded with a UV-visible spectrophotometer (Agilent 8453, California, CA, USA). The size and zeta potential of the samples were analyzed with a Nanoparticle Size analyzer (Nano-ZS90X, Malvern, Malvern, UK).

3. Results and Discussion

3.1. Quantification of Hydroxyl Groups of Lignin

The hydroxyl groups of lignin was quantified by ^{31}P NMR according to the reported method [28]. Approximately 20 mg of lignin was placed in a 1 mL vial. Then, 500 μL of a prepared solution of anhydrous pyridine and $CDCl_3$ (1.6:1, v/v) was added and magnetically stirred. Subsequently, 100 μL of chromium (III) acetylacetonate (5 mg/mL, dissolved in pyridine/$CDCl_3$, 1.6:1, V/V) was added as a relaxation agent and 100 μL of cyclohexanol (30 mg/mL) was added as an internal standard. Finally, 85 μL of phosphitylation reagents was added. After stirring for 10 min, the resulting solution was transferred to a 5 mm NMR tube and tested by NMR spectrometer. The ^{31}P NMR spectrum of lignin was shown in Figure 2. The result indicated that the hydroxyl group of guaiacylwas the most abundant in the lignin that is 3.76 mmol/g based on lignin, followed by the aliphatic hydroxyl that was 2.82 mmol/g, the condensed phenolic hydroxyl that was 1.90 mmol/g, and the carboxyl group that was 0.63 mmol/g. More hydroxyl groups indicated the lignin nanoparticles dispersed more stably in water [18].

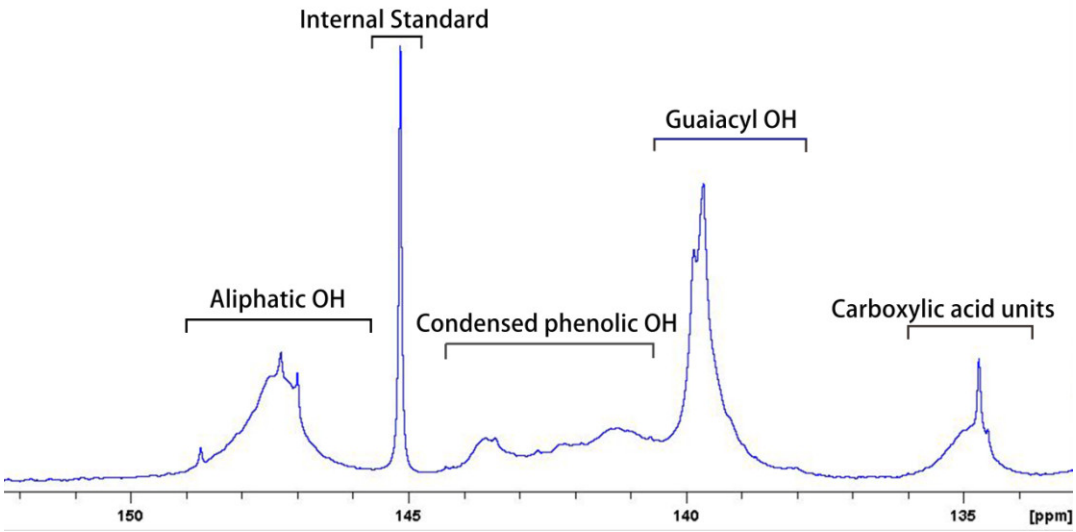

Figure 2. ^{31}P NMR spectra of the purified lignin.

3.2. Optimization of Fe_3O_4@LNPs Formation

The lignin hardly solubilized in water but dissolved in some organic solvents (e.g., THF). Therefore, Fe_3O_4NPs suspension used as the anti-solvent and THF used as the solvent were applied to prepare Fe_3O_4@LNPs through the lignin self-assembly. The initial concentration of lignin played a vital role in the morphology of lignin nanoparticles [29]. Figure 3 shows that Fe_3O_4@LNPs exhibited spherical shape. However, the size of Fe_3O_4@LNPs and its distribution varied with the initial concentration of lignin. Compared to L_1 prepared from 0.5 mg/mL lignin solution, L_2 and L_3 respectively prepared from 1.0 mg/mL and 5.0 mg/mL were more homogenous. Furthermore, L_2 had the highest load of Fe_3O_4 NPs.

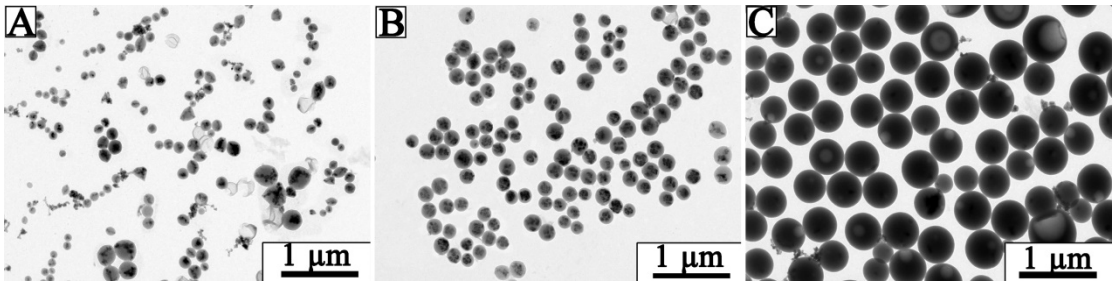

Figure 3. TEM images of Fe_3O_4@LNPs prepared by (**A**) L_1: 0.5 mg/mL, (**B**) L_2: 1.0 mg/mL, and (**C**) L_3: 5.0 mg/mL lignin.

The effect of lignin concentrations on the size and the size distribution of Fe_3O_4@LNPs were analyzed bydynamic light scattering (DLS). Figure 4 shows L_2 possessed a narrow size distribution with an average size of 152.8 nm. Compared to L_2, L_1 possessed a wide size distribution with an average size of 181.8 nm, and L_3 possessed a wide size distribution with an average size of 764.0 nm. The result indicated that 1.0 mg/mL was the optimum initial concentration of lignin for Fe_3O_4@LNPs preparation.

In the process of adding water droplets to the lignin/THF solution, lignin as an amphiphilic polymer, with its hydrophilic and hydrophobic properties, gradually aggregates and forms particles, which comprises the "nucleation growth mechanism" [18]. Figure 3 demonstrates that the morphology of the formed nanoparticle was impacted by the initial concentration of lignin. For example, 0.5 mg/mL lignin was applied, the average diameter of L_1 was only 181.8 nm but the size distribution was wide. The amount of lignin hardly meets the demand for the nanoparticles growth, resulting in the heterogeneous Fe_3O_4@LNPs (Figure 3A). However, when the high initial lignin concentration was applied, the extra lignin continued to aggregate on the surface of the formed

nanoparticles, eventually leading to the large size Fe_3O_4@LNPs (e.g., L_3) (Figure 3C). The homogeneous morphology of L_2 indicated that 1.0 mg/mL was the optimum concentration for Fe_3O_4@LNPs preparation (Figure 3B). The result was consistent with the previous report [30].

The surface charge of Fe_3O_4@LNPs was evaluated by the zeta potential. The results indicated that L_1, L_2, and L_3 possessed comparable negative zeta potentials of −29.2 mV, −32.4 mV and −32.4 mV, respectively, indicating that the initial lignin concentration had little effects on the surface charge of Fe_3O_4@LNPs. Therefore, L_1, L_2, and L_3 dispersed stably in aqueous solutions for an extended time without aggregation due to the electrical double layer repulsion induced from the protonation of phenolic hydroxyl and carboxyl groups of lignin. The comparable result was reported that LNPs dispersed stably in water for two months [18]. Based on the above results, L_2 was applied as the starting material for the further analysis in this study.

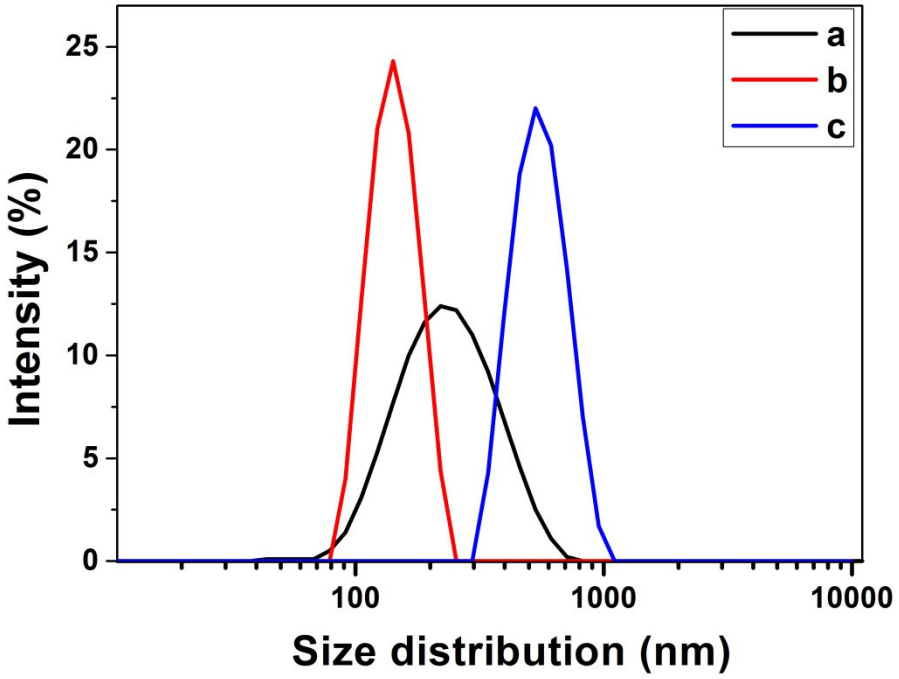

Figure 4. Size distribution of Fe_3O_4@LNPs prepared by (a) L_1: 0.5 mg/mL, (b) L_2: 1.0 mg/mL, and (c) L_3: 5mg/mL lignin.

3.3. Characterization of Fe_3O_4@LNPs

Fe_3O_4@LNPs surface possessed the negative charge which was explained as follows. The abundant hydroxyl and carboxyl groups of LNPs provide Fe_3O_4@LNPs surface a negative charge. In addition, when the hydrophobic surface of LNPs contacts with water, the hydroxyl ions are absorbed by the hydrophobic surface of LNPs, resulting the generation of strong negative zeta potential on the surface of Fe_3O_4@LNPs [18]. Therefore, Fe_3O_4 NPs loaded on LNPs can stabilize Fe_3O_4 NPs and prevent the aggregation of Fe_3O_4 NPs in solution.

The high resolution transmission electron microscope (HRTEM) image of individual Fe_3O_4@LNPs confirmed that Fe_3O_4NPs was loaded on the surface of LNPs (Figure 5A). The high-angle annular dark field (HAADF) image demonstrated the morphology of individual Fe_3O_4@LNPs, where C and Fe element respectively stands for LNPs and Fe_3O_4 NPs (Figure 5B and C). Thus, the HAADF and element mapping analysis confirmed the formation of Fe_3O_4@LNPs. The correlation of the size distribution of Fe_3O_4@LNPs and pH was investigated by DLS (Figure 6B). The result indicated that Fe_3O_4@LNPs had a narrow size distribution within pH from 3.0 to 10.5, confirming that Fe_3O_4@LNPs can stably disperse in aqueous solution with a wide pH range. This considerable dispersion ability of Fe_3O_4@LNPs was correlated with its zeta potential (approximately −30 mV) in solution within pH 3.0–10.5 (Figure 6C). When pH was below 3.0, the decrease of zeta potential induced the aggregation of Fe_3O_4@LNPs. On the other hand, when pH was above 11, the

surface charge decreased significantly which caused the aggregation of Fe_3O_4@LNPs enlarging the average diameter of nanoparticles. The surface charge of Fe_3O_4@LNPsdecreased with the increased concentration of Na^+ counter ions associated with the addition of NaOH for the pH adjustment. The result was consistent to the reported result on the dispersion stability of polymer nanoparticles correlated with the pH change [18,31].

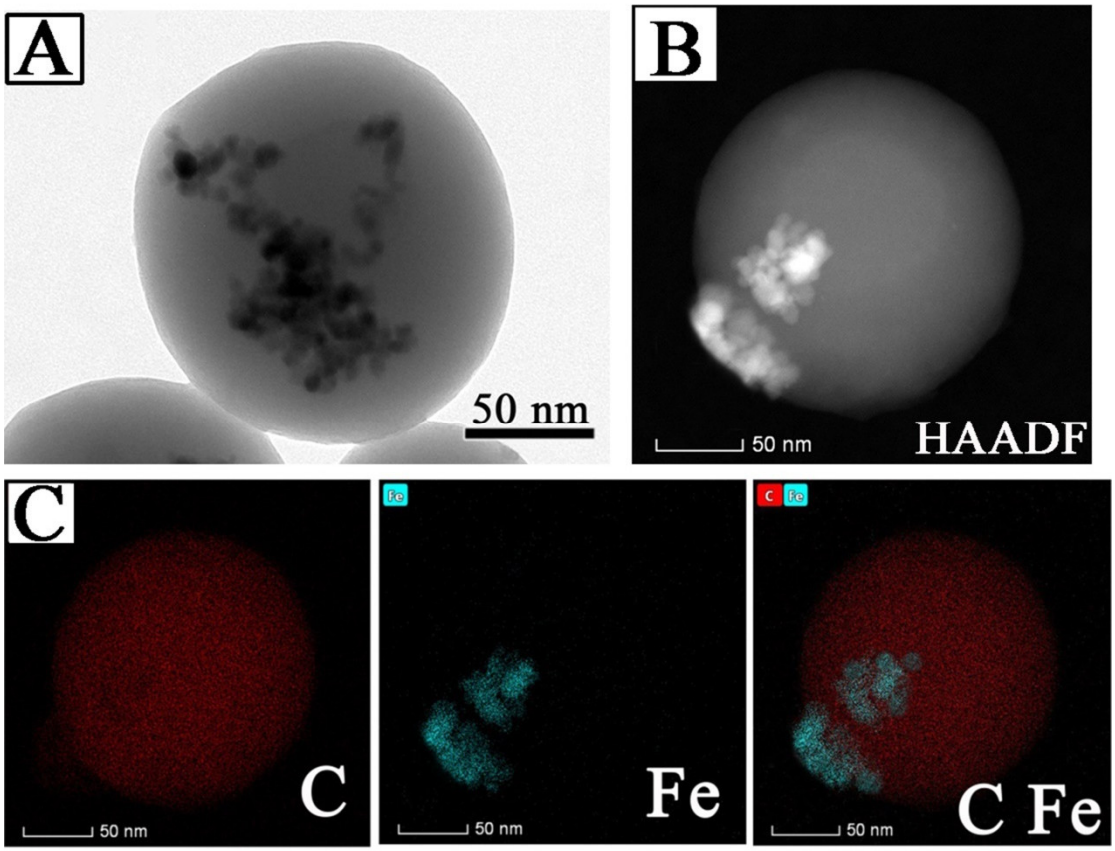

Figure 5. (**A**) HRTEM image of individual Fe_3O_4@LNPs; (**B**) High-angle annular dark field image (HAADF) and (**C**) element mapping analysis of Fe_3O_4@LNPs.

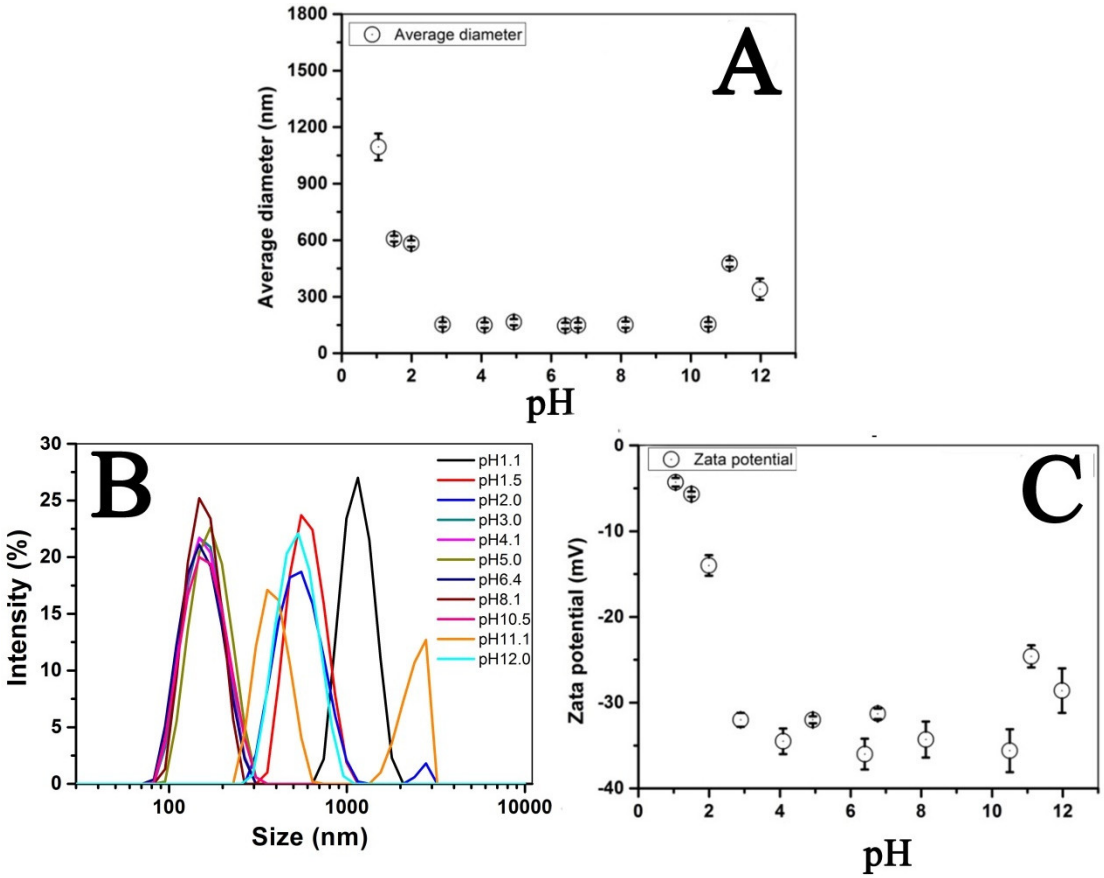

Figure 6. Effects of pH on (**A**) average size of Fe_3O_4@LNPs, (**B**) size distribution of Fe_3O_4@LNPs, and (**C**) zeta potential value of Fe_3O_4@LNPs.

3.4. Optimizing the Reaction Conditions of H_2O_2 and TMB Catalyzed by Fe_3O_4@LNPs

To improve the catalytic activity of Fe_3O_4@LNPs, the main parameters, e.g., time, pH, and temperature, were optimized. The experiment was performed as following 600 μL Fe_3O_4@LNPs (264 μg/mL), 300 μL TMB (4 mM) and 300 μL H_2O_2 (100 mM) were applied as reagents in 1.8 mL CPBS buffer solution (0.1 M). The relative activity of Fe_3O_4@LNPs with different pH, time and temperature were defined by follows: the maximum absorbance of the solution after reaction at 652 nm was set as 100%, and the relative activities were calculated by the equation: $R = (A/A_{max}) \times 100\%$, where R was the relative activity; A was the absorbance of the solution at 652 nm; and A_{max} was the maximum absorbance at 652 nm. The impacts of reaction time, pH, and temperature on the activity of Fe_3O_4@LNPs were demonstrated in Figure 7. The correlation between the reactivity of Fe_3O_4@LNPs and time was demonstrated in Figure 7A. It was shown that the activity of Fe_3O_4@LNPs increased to the maximum within 30 min. Thus, 30 min was set as the optimal reaction time for the following investigations. Within pH = 2.0–4.5, the Fe_3O_4@LNPs possessed a high and stable activity and achieved the maximum activity at pH = 3.0 (Figure 7B) that was contributed to solubilization of TMB in the acidic medium [32]. The comparable peroxidase-like activity were reported from HRP and other metal nanoenzymes [10,25]. The catalytic activity was significantly decreased when Fe_3O_4@LNPs was applied without the optimal pH (Figure 7B) because of the inherent defect of Fenton reaction [33]. It was reported that the catalytic activity of Fe_3O_4NPs loaded on multi-welled carbon nanotubes retained from pH 1–10 [33]; however the high cost of multi-welled carbon nanotubes limited its application. The catalytic activity of Fe_3O_4@LNPs was also impacted by temperature, and the maximum activity was achieved at 50 °C (Figure 7C). Compared to natural enzymes and Fe_3O_4 nanozymes [11], Fe_3O_4@LNPs retained the catalytic activity within a wide temperature range from 30 °C to 60 °C because of its considerable dispersion ability in the aqueous solution.

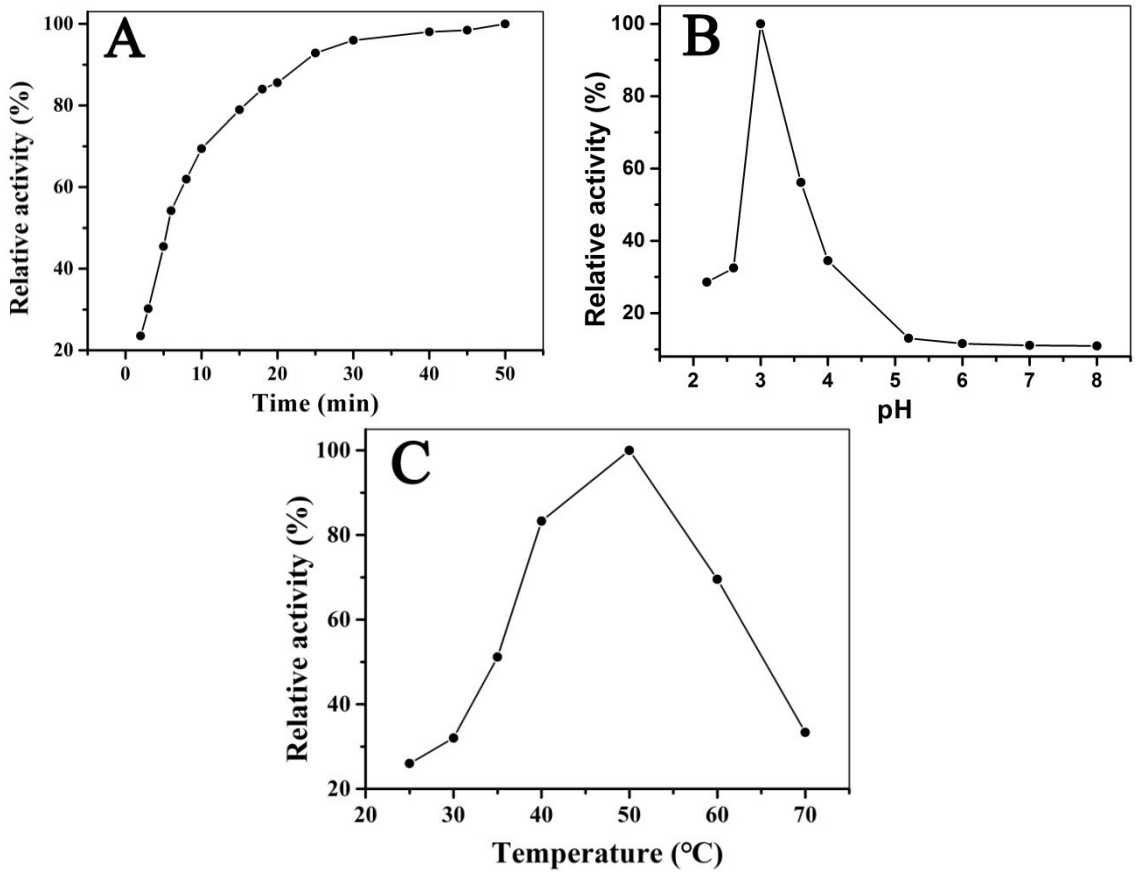

Figure 7. The catalytic activity of Fe_3O_4@LNPscorrelated with time (**A**), pH (**B**), and temperature (**C**).

3.5. Peroxidase-liked Activity of Fe_3O_4@LNPs

The peroxidase-liked activity of Fe_3O_4@LNPs was confirmed and evaluated by the reaction between TMB and H_2O_2 under optimal conditions. Little color changes and absorbance peaks at 652 nm were observed from the reaction of LNPs + TMB and LNPs + TMB + H_2O_2 (Figure 8 curve a and b), which suggested that LNPs possessed little catalytic activity. Little color change and absorbance peak at 652 nm were observed from the reaction of Fe_3O_4 NPs + TMB, confirming that TMB could not be oxidized without the presence of H_2O_2. The color change and absorbance peak at 652 nm were respectively observed from the reaction of Fe_3O_4 NPs + TMB + H_2O_2 and Fe_3O_4@LNPs + TMB + H_2O_2, which indicated TMB was oxidized during the reaction. However, the absorbance peak of Fe_3O_4@LNPs + TMB + H_2O_2 at 652 nm was significantly higher than that of Fe_3O_4 + TMB + H_2O_2, indicating Fe_3O_4@LNPs possessed stronger peroxidase-liked catalytic activity than Fe_3O_4 NPs due to its considerable dispersion ability. It was consistent with the reported result that Fe_3O_4 NPs stabilized by chitosan exhibited strong catalytic activity than Fe_3O_4 NPs [34].

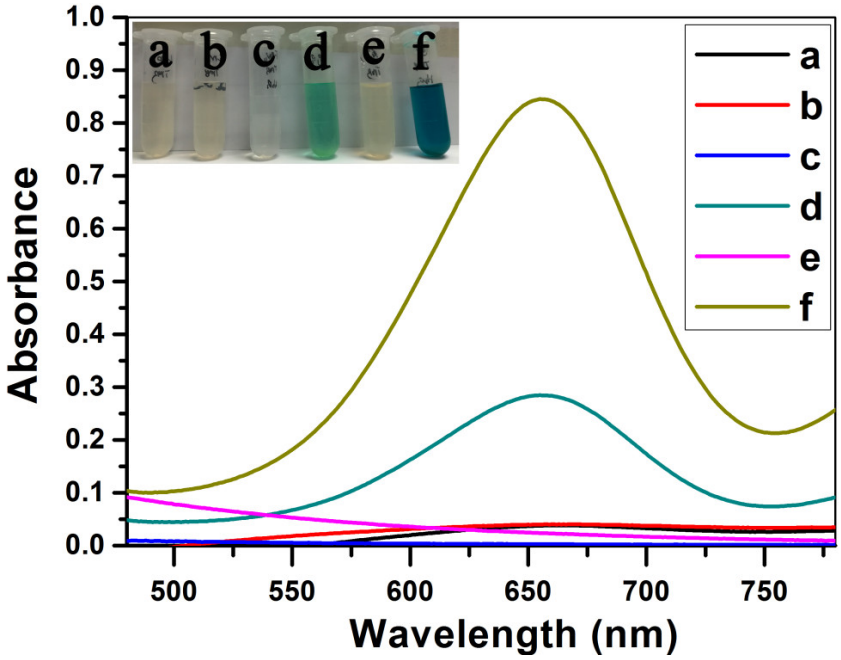

Figure 8. The UV-vis spectra of LNPs + TMB (a); LNPs + TMB + H_2O_2 (b); Fe_3O_4 + TMB (c); Fe_3O_4 + TMB + H_2O_2 (d); Fe_3O_4@LNPs + TMB (e) and Fe_3O_4@LNPs + TMB+ H_2O_2 (f); Insert is the photograph of the corresponding solution.

3.6. Steady-State Kinetic Study of Fe_3O_4@LNPs

The steady-state kinetic mechanism of Fe_3O_4@LNPsNPs reacted with H_2O_2 and TMB was investigated. The concentration of TMB-derived oxidation products was calculated by $A = \varepsilon \times b \times C$ (Beer-Lambert Law), where A is the absorbance value at 652 nm at room temperature and the molar absorption coefficient (ε) is 39,000 $M^{-1}cm^{-1}$ [35]. The Michaelis-Menten curves were obtained by following steps: the reaction rates of Fe_3O_4@LNPsNPs in different concentration of TMB or H_2O_2 were obtained by calculated the slope of the reaction system at 652 nm in the initial 5 min. Then, the reaction rates were plotted on the ordinate and the concentrations of TMB or H_2O_2 were plotted on the abscissa. The Lineweaver-Burk plots were obtained by taking the reciprocal of the reaction rate as the ordinate and the reciprocal of the concentration of TMB or H_2O_2. The reaction rate correlated with TMB concentration and H_2O_2 concentration was respectively demonstrated in Figure 9A and B. The Michaelis-Menten constant (K_m) is considered to be a key criterion for evaluating the enzyme's affinity to a substrate [32]. The maximum velocity (V_m) and K_m were obtained from the Lineweaver-Burk plots (Figure 9C and D) and summarized in Table 1. The K_m values of Fe_3O_4@LNPs towards TMB and H_2O_2 was comparable to that of HRP which indicated the Fe_3O_4@LNPsNPs could be used as an effective substitute for HRP. The K_m value of Fe_3O_4@LNPsNPs with TMB as the substrate was higher than that of Fe_3O_4 NPs with TMB, indicating that the Fe_3O_4 NPs have a higher affinity to TMB. The K_m value of the Fe_3O_4@LNPs with H_2O_2 was 29 times lower than that of the Fe_3O_4NPs with H_2O_2, suggesting that the Fe_3O_4@LNPs possessed significantly stronger affinity to H_2O_2 than the Fe_3O_4 NPs. However, the low K_m value of Fe_3O_4@LNPswith $H_2O_2$is potentially due to the continuous release of Fe_3O_4NPs from the Fe_3O_4@LNPs, thus avoiding the aggregation of Fe_3O_4 NPs and providing more reactive sites which enhanced the peroxidase-like activity of Fe_3O_4@LNPs during the reaction. The higher K_m value of Fe_3O_4NPs with H_2O_2 was consistent with the reported result that Fe_3O_4NPs needs a higher H_2O_2 concentration than Fe_3O_4@LNPs to obtain the comparable V_m [11]. Table 1 shows Fe_3O_4@LNPs possessed a comparable or stronger affinity to TMB or H_2O_2, compared to Fe_3O_4 NPs prepared by other methods [36–39]. Conclusively, the metal nanoparticles loaded on lignin nanoparticles improved its dispersion stability in solution and eventually increased its catalytic capacity.

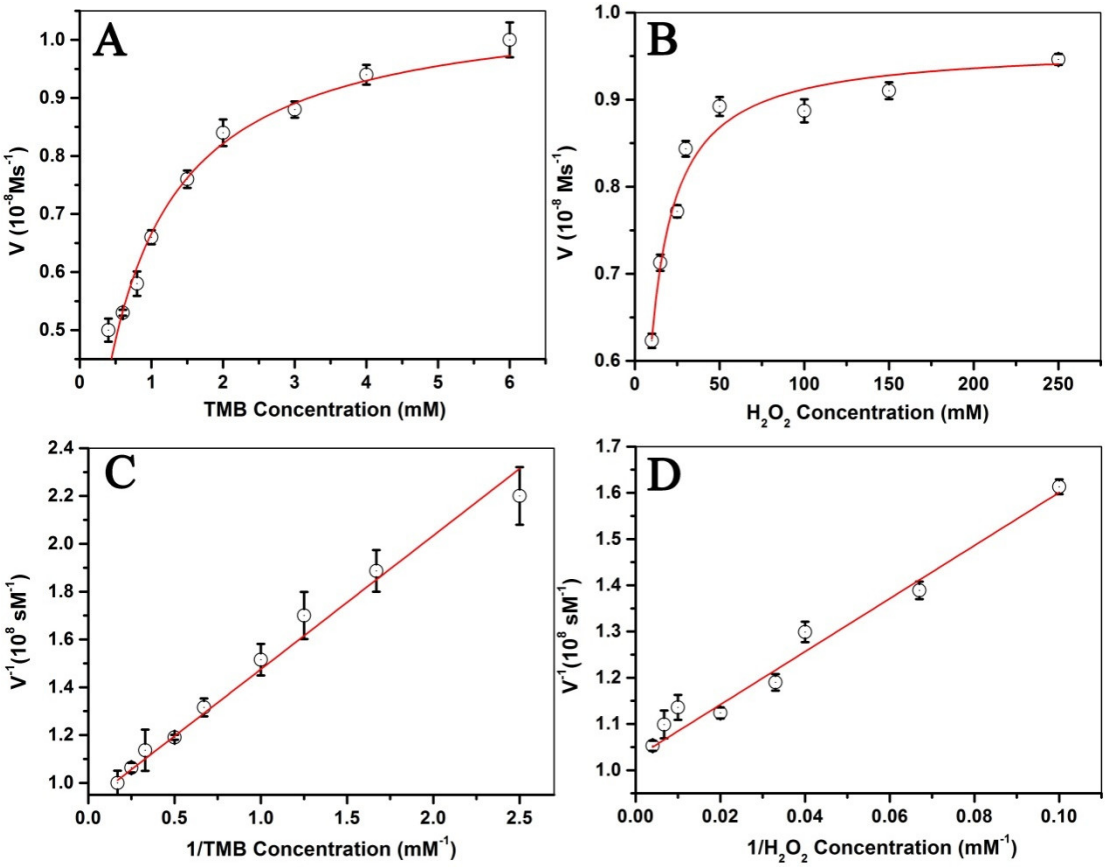

Figure 9. The steady-state dynamic analysis and catalytic mechanism of Fe_3O_4@LNPs: the Michaelis-Menten curves (**A** and **B**) and the double reciprocal plots of the activity of Fe_3O_4@LNPs(**C** and **D**).

Table 1. Comparisons of K_m and V_m among Fe_3O_4@LNPs, Fe_3O_4 NPs, and HRP.

Catalyst	Substrate	K_m/mM	$V_m/10^{-8}$ Ms^{-1}	Reference
Fe_3O_4@LNPs	TMB	0.51	1.03	This work
Fe_3O_4@LNPs	H_2O_2	5.30	0.96	This work
Fe_3O_4 NPs	TMB	0.01	3.44	[11]
Fe_3O_4 NPs	H_2O_2	154	9.78	[11]
HRP	TMB	0.43	10.00	[11]
HRP	H_2O_2	3.70	8.71	[11]
His-Fe_3O_4	H_2O_2	37.99	-	[37]
Ala-Fe_3O_4	H_2O_2	226.60	-	[37]
P-Fe_3O_4	TMB	0.44	-	[36]
CDs-Fe_3O_4	H_2O_2	56.97	-	[38]
GO-Fe_3O_4	H_2O_2	305.00	1.01	[40]

Note: His-Fe_3O_4: Histidine modified Fe_3O_4; Ala-Fe_3O_4: Alanine modified Fe_3O_4: Not given; P-Fe_3O_4: Porphyrin modified Fe_3O_4; CDs-Fe_3O_4: Carbon dots modified Fe_3O_4; GO-Fe_3O_4: Graphene oxide-based Fe_2O_3 hybrid.

3.7. The Colorimetric Detection of H_2O_2

Because the inherent peroxidase-like activity of Fe_3O_4@LNPs was H_2O_2 concentration dependent, a colorimetric method was designed to detect H_2O_2. Under the optimal conditions, in a total reaction volume of 3 mL, 264 μg/mL Fe_3O_4@LNPs and 4 mM TMB mixed with various concentrations of H_2O_2 in a CPBS buffer (pH = 3.0), the reaction was completed at 50 °C for 30 min. It was demonstrated in Figure 10A the solution color and the absorbance were correlated with H_2O_2

concentration. For example, the solution color became darker and the absorbance increased, as the concentration of H_2O_2 increased. The LOD of H_2O_2 concentration corresponding to the color variation was as low as 2 μM (Figure 10A, inset). When the concentration of H_2O_2 was less than 100 μM, there was a linear relationship between the absorbance at 652 nm and the H_2O_2 concentration. Conclusively, there was the possibility of the rapid detection of H_2O_2 by the naked eye or a UV-visible spectrophotometer when the Fe_3O_4@LNPs was applied.

The linear relationship between the absorbance at 652 nm and the H_2O_2 concentration was identified when the concentration of H_2O_2 ranged from 5 to 100 μM (Figure 10B). The linear regression equation was $A_{652nm} = 0.09993 + 0.00186C$ (where C is the concentration of H_2O_2), and the correlation coefficient (R^2) is 0.99077 (n = 3). The LODwas 2×10^{-6}M, which is lower than the counterpart of Fe_3O_4 NPs (3×10^{-6}M) [39].

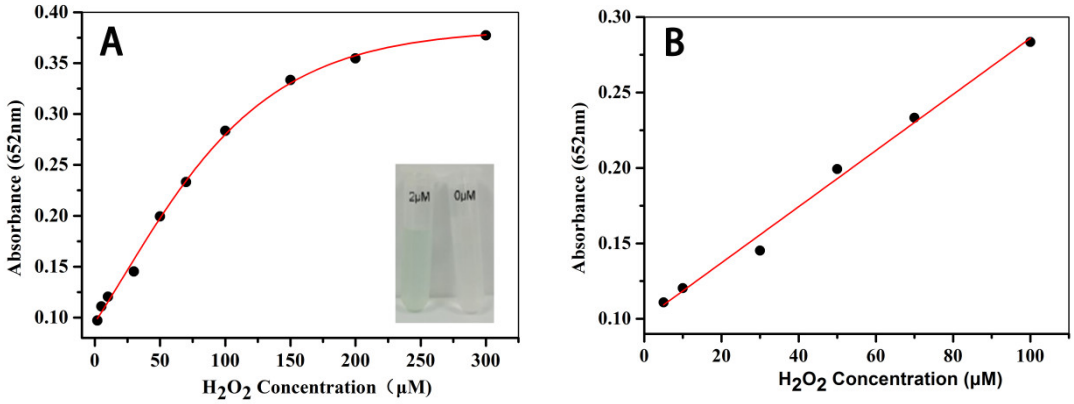

Figure 10. The dose-response curve for H_2O_2 detection (**A**), the inset: the colored products of different concentration of H_2O_2 (2 μM and 0 μM); the liner correlation between absorbance and H_2O_2 concentration (**B**).

4. Conclusion

Fe_3O_4@LNPs were prepared from the purified Spruce lignin using the self-assembly method. TEM and DLS analysis indicated that when the initial concentration of lignin solution was 1.0 mg/mL, the homogenous Fe_3O_4@LNPs was obtained, and the average size was 152.8 nm. The catalytic ability of Fe_3O_4@LNPs was optimized with the reaction time, pH, and temperature. Fe_3O_4@LNPs exhibited better peroxidase mimic activity than Fe_3O_4 NPs due to its more stable dispersion in the reaction system. The catalytic activity of Fe_3O_4@LNPs allows its colorimetric detection of H_2O_2 at 2 μM limitation of concentration.

Author Contributions: Q.Z., D.M., and S.W. originally conceived the idea and designed all the experiments. M.L., C.G., Z.J., and G.W. completed TEM, element mapping and DLS measurement. Q.Z., and D.M., wrote the manuscript. All the authors provided the discussion on the mechanism of Fe_3O_4@LNPs and reviewed the manuscript.

Funding: This research was funded by Postdoctoral Fund of China [2015M570419], Natural Science Fund of China [31400514], South China University of Technology Pulp and Paper Engineering State Key Laboratory Open Fund [2015016], and Guangxi University Guangxi Key Laboratory of Clean Pulp & Papermaking and Pollution Control Open Fund [ZR201805-7].

Conflicts of Interest: The authors declare no conflict of interest.

References

1. Muralikrishna, S.; Cheunkar, S.; Lertanantawong, B.; Ramakrishnappa, T.; Nagaraju, D.H.; Surareungchai, W.; Balakrishna, R.G.; Reddy, K.R. Graphene oxide-Cu(II) composite electrode for non-enzymatic determination of hydrogen peroxide. *J.Electroanal.Chem.***2016**, *776*, 59–65.

2. Zhang, X.; Bi, X.; Di, W.; Qin, W. A simple and sensitive $Ce(OH)CO_3/H_2O_2$/TMB reaction system for colorimetric determination of H_2O_2 and glucose. *Sens.ActuatorsBChem.***2016**, *231*, 714–722.
3. Sun, L.; Ding, Y.; Jiang, Y.; Liu, Q. Montmorillonite-loaded ceria nanocomposites with superior peroxidase-like activity for rapid colorimetric detection of H_2O_2. *Sens.ActuatorsBChem.***2017**, *239*, 848–856.
4. Zhang, Y.T.; Bai, S.J. An Improved Method for Determination of Trace Hydrogen Peroxide in Water. *J.Environ.Health***2006**, *23*, 258–261.
5. Sun, J.; Li, C.; Qi, Y.; Guo, S.; Liang, X. Optimizing Colorimetric Assay Based on V_2O_5 Nanozymes for Sensitive Detection of H_2O_2 and Glucose. *Sensors***2016**, *16*, 584.
6. Chen, Y.H. Determination of Peroxides in Food Samples by High Performance Liquid Chromatography with Variable Wavelength Detector. *Chin.J.Spectrosc.Lab.***2009**, *26*, 414–417.
7. Nasir, M.; Nawaz, M.H.; Latif, U.; Yaqub, M.; Hayat, A.; Rahim, A. An overview on enzyme-mimicking nanomaterials for use in electrochemical and optical assays. *Microchim.Acta***2016**, doi:10.1007/s00604-016-2036-8.
8. Sheng, Y.; Yang, H.; Wang, Y.; Han, L.; Zhao, Y.; Fan, A. Silver nanoclusters-catalyzed luminol chemiluminescence for hydrogen peroxide and uric acid detection. *Talanta***2017**, *166*, 268–274.
9. Han, L.; Zhang, H.; Chen, D.; Li, F. Protein-Directed Metal Oxide Nanoflakes with Tandem Enzyme-Like Characteristics: Colorimetric Glucose Sensing Based on One-Pot Enzyme-Free Cascade Catalysis. *Adv.Funct.Mater.***2018**, *28*, 1800018.
10. Zhao, K.; Gu, W.; Zheng, S.; Zhang, C.; Xian, Y. SDS–MoS_2 nanoparticles as highly-efficient peroxidase mimetics for colorimetric detection of H_2O_2 and glucose. *Talanta***2015**, *141*, 47–52.
11. Gao, L.; Zhuang, J.; Nie, L.; Zhang, J.; Zhang, Y.; Gu, N.; Wang, T.; Feng, J.; Yang, D.; Perrett, S. Intrinsic peroxidase-like activity of ferromagnetic nanoparticles. *Nat.Nanotechnol.***2007**, *2*, 577–583.
12. Asati, A.; Santra, S.; Kaittanis, C.; Nath, S.; Perez, J.M. Oxidase-like activity of polymer-coated cerium oxide nanoparticles. *Angew.Chem.***2009**, *48*, 2308–2312.
13. Liu, Q.; Yang, Y.; Li, H.; Zhu, R.; Shao, Q.; Yang, S.; Xu, J. NiO nanoparticles modified with 5,10,15,20-tetrakis(4-carboxyl pheyl)-porphyrin: Promising peroxidase mimetics for H_2O_2 and glucose detection. *Biosens.Bioelectron.***2015**, *64*, 147–153.
14. Liu, J.; Meng, L.; Fei, Z.; Dyson, P.J.; Jing, X.; Liu, X. MnO_2 nanosheets as an artificial enzyme to mimic oxidase for rapid and sensitive detection of glutathione. *Biosens.Bioelectron.***2017**, *90*, 69–74.
15. Ning, L.Y.; Guan, X.L.; Ma, J.W.; Wang, M.; Fan, X.B.; Zhang, G.L.; Zhang, F.B.; Peng, W.C.; Li, Y. A highly sensitive nonenzymatic H_2O_2 sensor based on platinum, $ZnFe_2O_4$ functionalized reduced graphene oxide. *J.Alloy.Compd.***2018**, *738*, 317–322, doi:10.1016/j.jallcom.2017.12.161.
16. Yang, X.; Ouyang, Y.J.; Wu, F.; Hu, Y.J.; Zhang, H.F.; Wu, Z.Y. In situ controlled preparation of platinum nanoparticles dopping into graphene sheets@cerium oxide nanocomposites sensitized screen printed electrode for nonenzymatic electrochemical sensing of hydrogen peroxide. *J.Electroanal.Chem.***2016**, *777*, 85–91, doi:10.1016/j.jelechem.2016.08.008.
17. Khan, M.E.; Khan, M.M.; Cho, M.H. Defected graphene nano-platelets for enhanced hydrophilic nature and visible light-induced photoelectrochemical performances. *J.Phys.Chem.Solids***2017**, *104*, 233–242, doi:10.1016/j.jpcs.2017.01.027.
18. Lievonen, M.; Valle-Delgado, J.J.; Mattinen, M.L.; Hult, E.L.; Lintinen, K.; Kostiainen, M.A.; Paananen, A.; Szilvay, G.R.; Setälä, H.; Österberg, M. Simple process for lignin nanoparticle preparation. *GreenChem.***2016**, *18*, 1416–1422.
19. Ragauskas, A.J.; Beckham, G.T.; Biddy, M.J.; Chandra, R.; Chen, F.; Davis, M.F.; Davison, B.H.; Dixon, R.A.; Gilna, P.; Keller, M. Lignin valorization: Improving lignin processing in the biorefinery. *Science***2014**, *344*, 1246843.
20. Hilgers, R.; Vincken, J.-P.; Gruppen, H.; Kabel, M.A. Laccase/Mediator Systems: Their Reactivity toward Phenolic Lignin Structures. *ACSSustain.Chem.Eng.***2018**, *6*, 2037–2046, doi:10.1021/acssuschemeng.7b03451.
21. Zhang, H.; Bai, Y.; Zhou, W.; Chen, F. Color reduction of sulfonated eucalyptus kraft lignin. *Int.J.Biol.Macromol.***2017**, *97*, 201–208.
22. Chang, Q.; Deng, K.; Zhu, L.; Jiang, G.; Yu, C.; Tang, H. Determination of hydrogen peroxide with the aid of peroxidase-like Fe_3O_4 magnetic nanoparticles as the catalyst. *Microchim.Acta***2009**, *165*, 299.
23. Jiang, B.; Duan, D.; Gao, L.; Zhou, M.; Fan, K.; Tang, Y.; Xi, J.; Bi, Y.; Tong, Z.; Gao, G.F.; et al. Standardized assays for determining the catalytic activity and kinetics of peroxidase-like nanozymes. *Nat.Protoc.***2018**, *13*, 1506–1520, doi:10.1038/s41596-018-0001-1.

24. Zhu, M.; Dai, Y.; Wu, Y.; Liu, K.; Qi, X.; Sun, Y. Bandgap control of alpha-Fe_2O_3 nanozymes and their superior visible light promoted peroxidase-like catalytic activity. *Nanotechnology***2018**, *29*, 465704, doi:10.1088/1361-6528/aaddc2.
25. Ding, Y.; Yang, B.; Liu, H.; Liu, Z.; Zhang, X.; Zheng, X.; Liu, Q. FePt-Au ternary metallic nanoparticles with the enhanced peroxidase-like activity for ultrafast colorimetric detection of H_2O_2. *Sens.ActuatorsBChem.***2018**, *259*, 775–783.
26. Liu, Q.; Zhang, L.; Li, H.; Jia, Q.; Jiang, Y.; Yang, Y.; Zhu, R. One-pot synthesis of porphyrin functionalized γ-Fe_2O_3 nanocomposites as peroxidase mimics for H_2O_2 and glucose detection. *Mater.Sci.Eng.C***2015**, *55*, 193–200.
27. Chen, Y.; Xianyu, Y.; Dong, M.; Zhang, J.; Zheng, W.; Qian, Z.; Jiang, X. Cascade Reaction-Mediated Assembly of Magnetic/Silver Nanoparticles for Amplified Magnetic Biosensing. *Anal.Chem.***2018**, *90*, 6906–6912, doi:10.1021/acs.analchem.8b01138.
28. Zhao, W.; Xiao, L.P.; Song, G.; Sun, R.C.; He, L.; Singh, S.; Simmons, B.A.; Cheng, G. From lignin subunits to aggregates: Insights into lignin solubilization. *GreenChem.***2017**, *19*, 3272–3281.
29. Xiong, F.; Han, Y.; Wang, S.; Li, G.; Qin, T.; Chen, Y.; Chu, F. Preparation and Formation Mechanism of Renewable Lignin Hollow Nanospheres with a Single Hole by Self-Assembly. *AcsSustain.Chem.Eng.***2017**, *5*, 2273–2281, doi:10.1021/acssuschemeng.6b02585.
30. Destrée, C.; B.Nagy, J. Mechanism of formation of inorganic and organic nanoparticles from microemulsions. *Adv.ColloidInterfaceSci.***2006**, *123–126*, 353–367.
31. Ishikawa, Y.; Katoh, Y.; Ohshima, H. Colloidal stability of aqueous polymeric dispersions: Effect of pH and salt concentration. *ColloidsSurf.B-Biointerfaces***2005**, *42*, 53–58, doi:10.1016/j.colsurfb.2005.01.006.
32. Liu, H.; Jiao, M.; Gu, C.; Zhang, M. Au@CuxOS yolk-shell nanomaterials with porous shells act as a new peroxidase mimic for the colorimetric detection of H_2O_2. *J.Alloy.Compd.***2017**, *741*, 197–204.
33. Wang, H.; Jiang, H.; Wang, S.; Shi, W.; He, J.; Liu, H.; Huang, Y. Fe_3O_4–MWCNT magnetic nanocomposites as efficient peroxidase mimic catalysts in a Fenton-like reaction for water purification without pH limitation. *RscAdv.***2014**, *4*, 45809–45815.
34. Jiang, J.; He, C.; Wang, S.; Jiang, H.; Li, J.; Li, L. Recyclable ferromagnetic chitosan nanozyme for decomposing phenol. *Carbohydr.Polym.***2018**, *198*, 348–353, doi:10.1016/j.carbpol.2018.06.068.
35. Ding, Y.; Fan, F.R.; Tian, Z.Q.; Wang, Z.L. Sublimation-Induced Shape Evolution of Silver Cubes. *Small***2009**, *5*, 2812–2815, doi:10.1002/smll.200901189.
36. Liu, Q.Y.; Li, H.; Zhao, Q.R.; Zhu, R.R.; Yang, Y.T.; Jia, Q.Y.; Bian, B.; Zhuo, L.H. Glucose-sensitive colorimetric sensor based on peroxidase mimics activity of porphyrin-Fe(3)O(4) nanocomposites. *Mater.Sci.Eng.C-Mater.Biol.Appl.***2014**, *41*, 142–151, doi:10.1016/j.msec.2014.04.038.
37. Fan, K.; Wang, H.; Xi, J.; Liu, Q.; Meng, X.; Duan, D.; Gao, L.; Yan, X. Optimization of Fe_3O_4 nanozyme activity via single amino acid modification mimicking an enzyme active site. *Chem.Commun.***2016**, *53*, 424–427, doi:10.1039/c6cc08542c.
38. Chen, S.; Chi, M.; Yang, Z.; Gao, M.; Wang, C.; Lu, X. Carbon dots/Fe_3O_4 hybrid nanofibers as efficient peroxidase mimics for sensitive detection of H_2O_2 and ascorbic acid. *Inorg.Chem.Front.***2017**, *4*, 1621–1627, doi:10.1039/c7qi00308k.
39. Hui, W.; Erkang, W. Fe_3O_4 magnetic nanoparticles as peroxidase mimetics and their applications in H_2O_2 and glucose detection. *Anal.Chem.***2008**, *80*, 2250–2254,doi:10.1021/ac702203f.
40. Song, L.; Huang, C.; Zhang, W.; Ma, M.; Chen, Z.; Gu, N.; Zhang, Y. Graphene oxide-based Fe_2O_3 hybrid enzyme mimetic with enhanced peroxidase and catalase-like activities. *ColloidsSurf.APhysicochem.Eng.Asp.***2016**, *506*, 747–755, doi:10.1016/j.colsurfa.2016.07.037.